JCI insight

NOX4 modulates macrophage phenotype and mitochondrial biogenesis in asbestosis

Chao He, … , Linlin Gu, A. Brent Carter

JCI Insight. 2019;4(16):e126551. https://doi.org/10.1172/jci.insight.126551.

Research Article | Immunology | Pulmonology

Graphical abstract

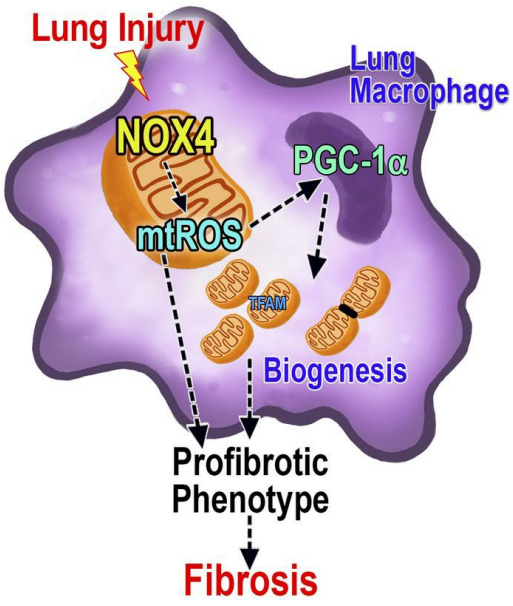

JCI insight

RESEARCH ARTICLE

NOX4 modulates macrophage phenotype and mitochondrial biogenesis in asbestosis

Chao He,[1] Jennifer L. Larson-Casey,[1] Dana Davis,[1] Vidya Sagar Hanumanthu,[2] Ana Leda F. Longhini,[2] Victor J. Thannickal,[1,3] Linlin Gu,[1] and A. Brent Carter[1,3]

[1]Department of Medicine, Division of Pulmonary, Allergy and Critical Care Medicine, and [2]Division of Clinical Immunology and Rheumatology, University of Alabama at Birmingham, Birmingham, Alabama, USA. [3]Birmingham Veterans Administration Medical Center, Birmingham, Alabama, USA.

Macrophage activation is implicated in the development of pulmonary fibrosis by generation of profibrotic molecules. Although NADPH oxidase 4 (NOX4) is known to contribute to pulmonary fibrosis, its effects on macrophage activation and mitochondrial redox signaling are unclear. Here, we show that NOX4 is crucial for lung macrophage profibrotic polarization and fibrotic repair after asbestos exposure. NOX4 was elevated in lung macrophages from subjects with asbestosis, and mice harboring a deletion of NOX4 in lung macrophages were protected from asbestos-induced fibrosis. NOX4 promoted lung macrophage profibrotic polarization and increased production of profibrotic molecules that induce collagen deposition. Mechanistically, NOX4 further augmented mitochondrial ROS production and induced mitochondrial biogenesis. Targeting redox signaling and mitochondrial biogenesis prevented the profibrotic polarization of lung macrophages by reducing the production of profibrotic molecules. These observations provide evidence that macrophage NOX4 is a potentially novel therapeutic target to halt the development of asbestos-induced pulmonary fibrosis.

Introduction

Macrophages are believed to contribute to various fibrotic disease processes by increasing the generation of profibrotic cytokines and production of collagen synthesis substrates, such as proline, and molecules implicated in extracellular matrix dynamics (1). Macrophages produce high levels of ROS, including H_2O_2, which has a critical role in the pathogenesis of pulmonary fibrosis (2). We have shown that mitochondrial ROS production can promote profibrotic polarization of macrophages (3–5).

NADPH oxidase 4 (NOX4) belongs to a family of enzymes named nicotinamide adenine dinucleotide phosphate hydrogen (NADPH) oxidases, whose primary function is catalyzing the reduction of oxygen to superoxide anion free radicals (6). NOX enzymes are located primarily within the cell or phagosome membranes; however, NOX4 is localized in mitochondria (7, 8). Another unique property of NOX4 is that it generates H_2O_2 in addition to superoxide radicals. Previous studies indicate that NOX4 contributes to pulmonary fibrosis development because NOX4 expression is elevated in whole lung homogenates after bleomycin exposure (9, 10). Additionally, administration of NOX4 siRNA intratracheally after bleomycin exposure attenuates fibrogenesis. The effect of NOX4 on fibrosis development has been proposed to be mediated by its effects on fibroblast activation and alveolar epithelial cell apoptosis. The effects of NOX4 in myeloid cells in fibrotic repair are not known.

Emerging evidence suggests that mitochondria play a crucial role in pulmonary fibrosis development (11–13). A dynamic process involving both mitophagy and mitochondrial biogenesis maintains mitochondrial homeostasis; however, mitochondrial homeostasis is typically disrupted during fibrosis development. We have shown that mitophagy was increased in lung macrophages from fibrotic subjects and bleomycin-injured mice, and mitophagy was necessary for apoptosis resistance (12). Other groups have shown that mitochondrial biogenesis is reduced in alveolar epithelial type II cells and fibroblasts after bleomycin exposure (13, 14). Restoring mitochondrial homeostasis by increasing biogenesis in either alveolar epithelial type II cells or fibroblasts has been proposed to ameliorate pulmonary fibrosis. So far, neither NOX4 nor

Conflict of interest: The authors have declared that no conflict of interest exists.

Submitted: December 3, 2018
Accepted: July 16, 2019
Published: August 22, 2019.

Reference information: *JCI Insight*. 2019;4(16):e126551. https://doi.org/10.1172/jci.insight.126551.

the presence of mitochondrial biogenesis in lung macrophages during pulmonary fibrosis development has been evaluated, and it is not known whether targeting this pathway in macrophages may be beneficial. Our data show that NOX4 was elevated in fibrotic lung macrophages, which led to increased H_2O_2 production and profibrotic polarization of macrophages. These macrophages had augmented mitochondrial biogenesis that is critical for phenotypic switching and asbestos-induced pulmonary fibrosis development.

Results

NOX4 expression in lung macrophages contributes to asbestos-induced pulmonary fibrosis development. To determine whether NOX4 has a role in macrophages during fibrosis, we measured *NOX4* gene expression in lung macrophages isolated from normal subjects and subjects with asbestosis. Lung macrophages isolated from subjects with asbestosis had increased *NOX4* expression compared with healthy subjects (Figure 1A). The expression of NOX4 was localized to the mitochondria of lung macrophages from subjects with asbestosis and was greater than 3-fold more compared with normal subjects (Figure 1, B and C). Similar observations were seen in WT mice exposed to chrysotile asbestos intratracheally. Lung macrophages from WT mice exposed to chrysotile asbestos had increased mitochondrial NOX4 expression compared with WT mice exposed to vehicle (Supplemental Figure 1, A and B; supplemental material available online with this article; https://doi.org/10.1172/jci.insight.126551DS1). In vitro, asbestos treatment increased mitochondrial NOX4 content in macrophages (Supplemental Figure 1C).

To validate these observations in vivo, WT and *Nox4*$^{-/-}$ mice were exposed to chrysotile asbestos intratracheally. *Nox4*$^{-/-}$ mice were protected from developing fibrosis and had significantly decreased collagen deposition compared with WT mice (Figure 1, D and E). To determine the effect of NOX4 specifically in macrophages, we generated mice harboring a deletion of NOX4 in macrophages (*Nox4*$^{-/-}$*Lyz2-Cre*). The predominant cell type in the bronchoalveolar lavage (BAL) fluid on day 21 was macrophages (Supplemental Figure 1D). *Nox4*$^{-/-}$*Lyz2-Cre* mice were protected from developing pulmonary fibrosis and had less collagen content, similar to the MMVF control (Figure 1, F and G). *Nox4*$^{-/-}$*Lyz2-Cre* mice lacked NOX4 expression in lung macrophages (Figure 1G, inset) but not in alveolar epithelial cells (Supplemental Figure 1E).

Recent data have highlighted a role of monocyte-derived macrophages in the development of pulmonary fibrosis (15). Using flow cytometry (Supplemental Figure 1F), we found an increased number of monocyte-derived macrophages (MDMs) after asbestos exposure in *Nox4*$^{fl/fl}$ mice, whereas the number of tissue-resident macrophages (TRMs) decreased (Figure 1, H and I). The number of MDMs and TRMs remained unchanged after asbestos exposure in the *Nox4*$^{-/-}$*Lyz2-Cre* mice (Figure 1, H and I), suggesting one potential mechanism by which these mice are protected from asbestos-induced pulmonary fibrosis.

To highlight the importance of MDMs, liposomal clodronate (clodrosome) was administered intratracheally to deplete TRMs as previously described (15). Three days after clodrosome treatment, most of the TRMs were depleted (Supplemental Figure 1G). Clodrosome treatment does not alter the course of fibrosis development in asbestos-exposed mice, suggesting that MDMs, not TRMs, are the main driver for fibrosis (Supplemental Figure 1H). Together, these data demonstrate that NOX4 in lung macrophages, particularly MDMs, has a critical role in fibrotic repair and that targeting NOX4 may protect from fibrosis development.

NOX4 mediates profibrotic polarization of lung macrophages. We have previously shown that lung macrophages from subjects with asbestosis have increased profibrotic markers (5). Similarly, expression of profibrotic genes *tgfb1*, *arginase 1*, and *il10* was elevated in lung macrophages from subjects with asbestosis (Figure 2, A–C). The reverse was seen in expression of proinflammatory genes *inos* and *tnfa*, which was decreased in lung macrophages from subjects with asbestosis (Supplemental Figure 2, A and B). Because profibrotic phenotypic switching of macrophages contributes to fibrosis development, we measured 2 profibrotic cytokines in the BAL fluid from *Nox4*$^{fl/fl}$ and *Nox4*$^{-/-}$*Lyz2-Cre* mice after asbestos exposure. *Nox4*$^{-/-}$*Lyz2-Cre* mice had nearly 3-fold decreased active TGF-β_1 (Figure 2D) and significantly decreased Ym-1 in the BAL fluid compared with *Nox4*$^{fl/fl}$ mice (Figure 2E). We used FACS analysis to determine the specific number of profibrotic and proinflammatory macrophages in the BAL. *Nox4*$^{-/-}$*Lyz2-Cre* mice had a significant decrease in CD206 and CD163 expression compared with *Nox4*$^{fl/fl}$ mice; however, CD86 and MHC II expression was similar in both strains of mice (Supplemental Figure 2C), suggesting that NOX4 regulates profibrotic polarization only.

To support our in vivo observations, transfection of NOX4 led to a significant increase of several signature profibrotic genes, including *fizz1* (Figure 2F), *ym1* (Figure 2G), and *tgfb1* (Figure 2H). Bone marrow–derived macrophages (BMDMs) from *Nox4*$^{-/-}$ mice had significantly reduced levels of profibrotic gene expression, including *fizz1* (Figure 2I), *ym1* (Figure 2J), and *tgfb1* (Figure 2K) compared with

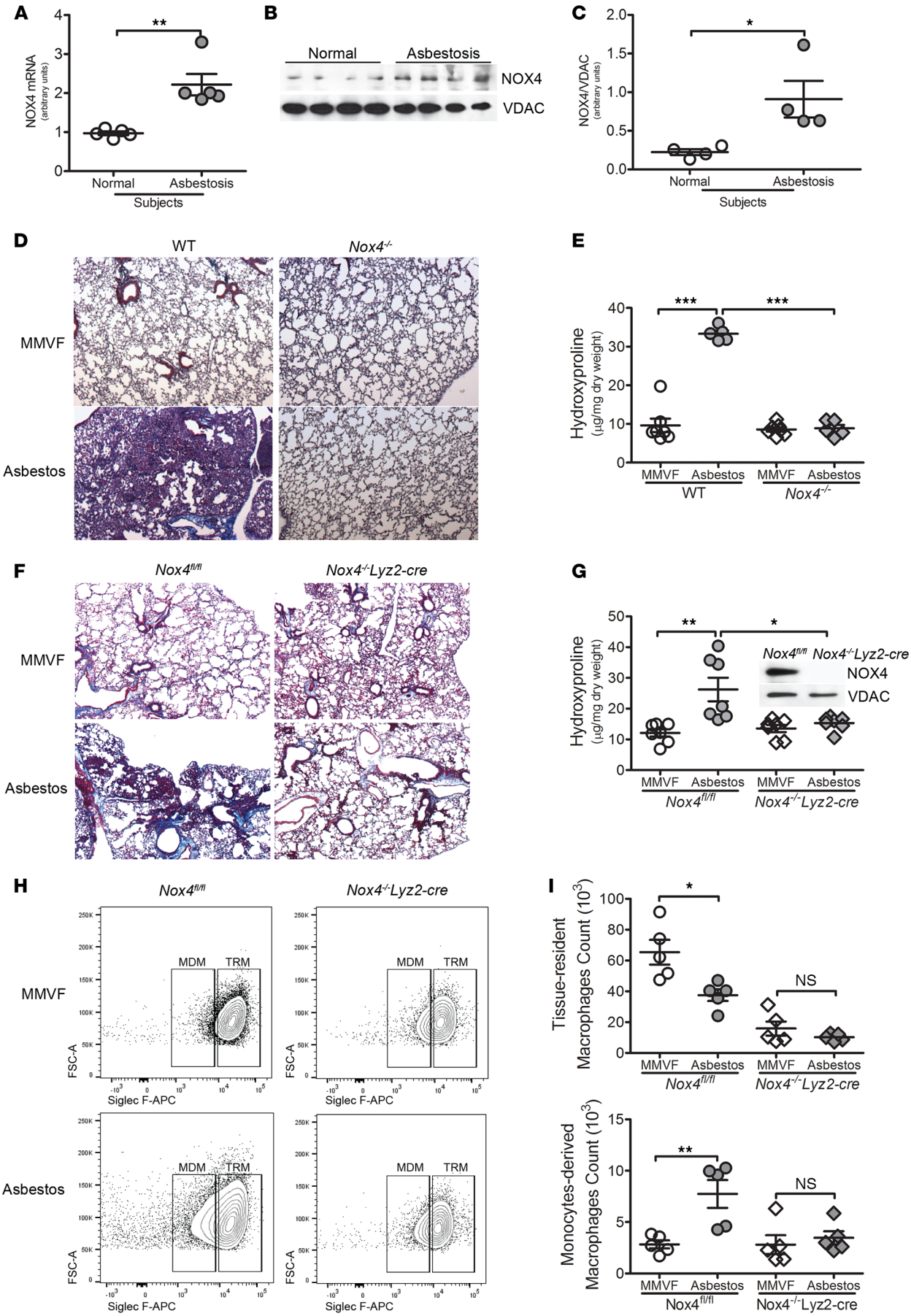
A
NOX4 mRNA (arbitrary units)
Normal
Asbestosis
Subjects
B
Normal
Asbestosis
NOX4
VDAC
C
NOX4/VDAC (arbitrary units)
Normal
Asbestosis
Subjects
D
WT
Nox4-/-
MMVF
Asbestos
E
Hydroxyproline (μg/mg dry weight)
MMVF
Asbestos
WT
Nox4-/-
F
Nox4fl/fl
Nox4-/-Lyz2-cre
MMVF
Asbestos
G
Hydroxyproline (μg/mg dry weight)
Nox4fl/fl
Nox4-/-Lyz2-cre
NOX4
VDAC
H
Nox4fl/fl
Nox4-/-Lyz2-cre
MMVF
Asbestos
MDM
TRM
FSC-A
Siglec F-APC
I
Tissue-resident Macrophages Count (10^3)
Monocytes-derived Macrophages Count (10^3)
NS

Figure 1. NOX4 promotes fibrosis development. (**A**) *NOX4* mRNA expression in lung macrophages from normal (n = 5) or asbestosis subjects (n = 5). (**B**) Immunoblot analysis of NOX4 expression in isolated mitochondria from normal (n = 4) and asbestosis subjects (n = 4). (**C**) Quantification of mitochondrial NOX4 expression normalized to VDAC. (**D**) Representative histology of lung sections (n = 5) and (**E**) hydroxyproline analysis of homogenized lung (n = 5) from WT and *Nox4*$^{-/-}$ mice exposed to either man-made vitreous fibers (MMVFs) or chrysotile asbestos. (**F**) Representative histology of lung sections (n = 5) and (**G**) hydroxyproline analysis of homogenized lung (n = 7) from *Nox4*$^{fl/fl}$ and *Nox4*$^{-/-}$*Lyz2-Cre* mice exposed to either MMVF or chrysotile asbestos. Inset, immunoblot of NOX4 in bronchoalveolar lavage (BAL) cells from *Nox4*$^{fl/fl}$ and *Nox4*$^{-/-}$*Lyz2-Cre* mice. Original magnification, ×5. (**H**) Representative contour plot of lung macrophages in BAL (n = 5) from *Nox4*$^{fl/fl}$ and *Nox4*$^{-/-}$*Lyz2-Cre* mice exposed to either MMVF or chrysotile asbestos. (**I**) Numbers of monocyte-derived macrophages (MDMs) and tissue-resident macrophages (TRMs) in BAL (n = 5) from *Nox4*$^{fl/fl}$ and *Nox4*$^{-/-}$*Lyz2-Cre* mice exposed to either MMVF or chrysotile asbestos. *P < 0.05, **P < 0.01, ***P < 0.001. Values shown as mean ± SEM. Two-tailed t test or 1-way ANOVA followed by Tukey's multiple-comparisons test was used. Each dot represents 1 human subject, 1 animal, or 1 sample. All in vitro experiments, including Western blotting, were repeated independently thrice, and representative blots are shown.

WT macrophages. Likewise, deletion of NOX4 in BMDMs decreased active TGF-β_1 in conditioned media below the level of the WT control (Supplemental Figure 2D). Moreover, *Nox4*$^{-/-}$ macrophages had decreased arginase activity (Figure 2L), a key metabolic feature of profibrotic polarization. In aggregate, NOX4 is critical for macrophage activation to a profibrotic phenotype, and the absence of NOX4 reduces production of profibrotic markers, including TGF-β_1.

NOX4 promotes mitochondrial biogenesis in lung macrophages. NOX4 is reported to be located in mitochondria of macrophages and other cell types (7, 8, 16). We isolated whole mitochondria and mitoplasts (mitochondrial inner membrane and matrix) to verify that NOX4 is indeed in the mitochondria of lung macrophages (Supplemental Figure 3A). Mitochondrial dynamics play a pivotal role in the development of pulmonary fibrosis. NOX4 has been linked to mitochondrial dynamics (17), but the involvement of NOX4 in macrophages is not known. Peroxisome proliferator–activated receptor–γ coactivator 1-α (PGC-1α) is considered the central regulator of mitochondrial biogenesis (18). PGC-1α expression in alveolar epithelial cells is required to maintain mitochondrial homeostasis and prevent bleomycin-induced fibrotic repair in a murine model (14).

Subjects with asbestosis had more than 10-fold greater *pgc1a* expression compared with normal subjects (Figure 3A). Similarly, subjects with asbestosis had significantly increased mitochondrial transcription factor A (*tfam*) (Figure 3B). Subjects with asbestosis also had a significantly higher level of TFAM protein expression compared with normal subjects (Supplemental Figure 3B).

We questioned whether increased mitochondrial biogenesis is related to increased NOX4 expression. NOX4 overexpression resulted in significantly greater *pgc1a* (Figure 3C) and *tfam* (Figure 3D) expression compared with cells transfected with an empty vector, and expression increased significantly further with asbestos exposure. In addition, both *pgc1a* (Figure 3E) and *tfam* (Figure 3F) promoter activities had nearly a 10-fold increase in cells transfected with a NOX4 vector compared with empty vector–transfected cells. The reverse was seen in the absence of NOX4. BMDMs from *Nox4*$^{-/-}$ mice had decreased *pgc1a* and *tfam* expression compared with WT macrophages (Supplemental Figure 3C). To further support our observations, we measured mitochondrial DNA content. Macrophages overexpressing NOX4 had increased mitochondrial DNA (mtDNA) content, and the increase in mtDNA was enhanced by asbestos exposure (Figure 3G).

PGC-1α is known to be activated by p38 MAPK (19). NOX4 overexpression activates p38 in macrophages (Supplemental Figure 3D). Inhibition of p38 MAPK activity using a selective inhibitor, SB203580, was able to attenuate NOX4-induced *pgc1a* and *tfam* gene promoter activities (Supplemental Figure 3, E and F).

We asked whether mitochondrial biogenesis occurred during asbestos-induced fibrosis. We performed transmission electron microscopy to examine the number of mitochondria in lung macrophages. Asbestos-induced injury increased the number of mitochondria in lung macrophages in *Nox4*$^{fl/fl}$ mice, and the *Nox4*$^{fl/fl}$ mice had increased mitochondrial number compared with lung macrophages from *Nox4*$^{-/-}$*Lyz2-Cre* mice (Figure 3H). In addition, asbestos exposure did not alter mitochondrial number in *Nox4*$^{-/-}$*Lyz2-Cre* mice (Figure 3I). To relate this difference in mitochondrial number to biogenesis, *Nox4*$^{fl/fl}$ mice exposed to asbestos had increased *pgc1a* (Figure 3J) and *tfam* expression (Figure 3K), whereas lung macrophages from *Nox4*$^{-/-}$*Lyz2-Cre* mice were reduced to the level of the MMVF control. Other genes indicative of mitochondrial biogenesis, such as *cs* (Supplemental Figure 3G), *cox iv* (Supplemental Figure 3H), and *drp1* (Supplemental Figure 3I), showed a similar pattern. In aggregate, these observations indicate that mitochondrial biogenesis is NOX4 dependent and is increased during asbestos-induced fibrotic repair.

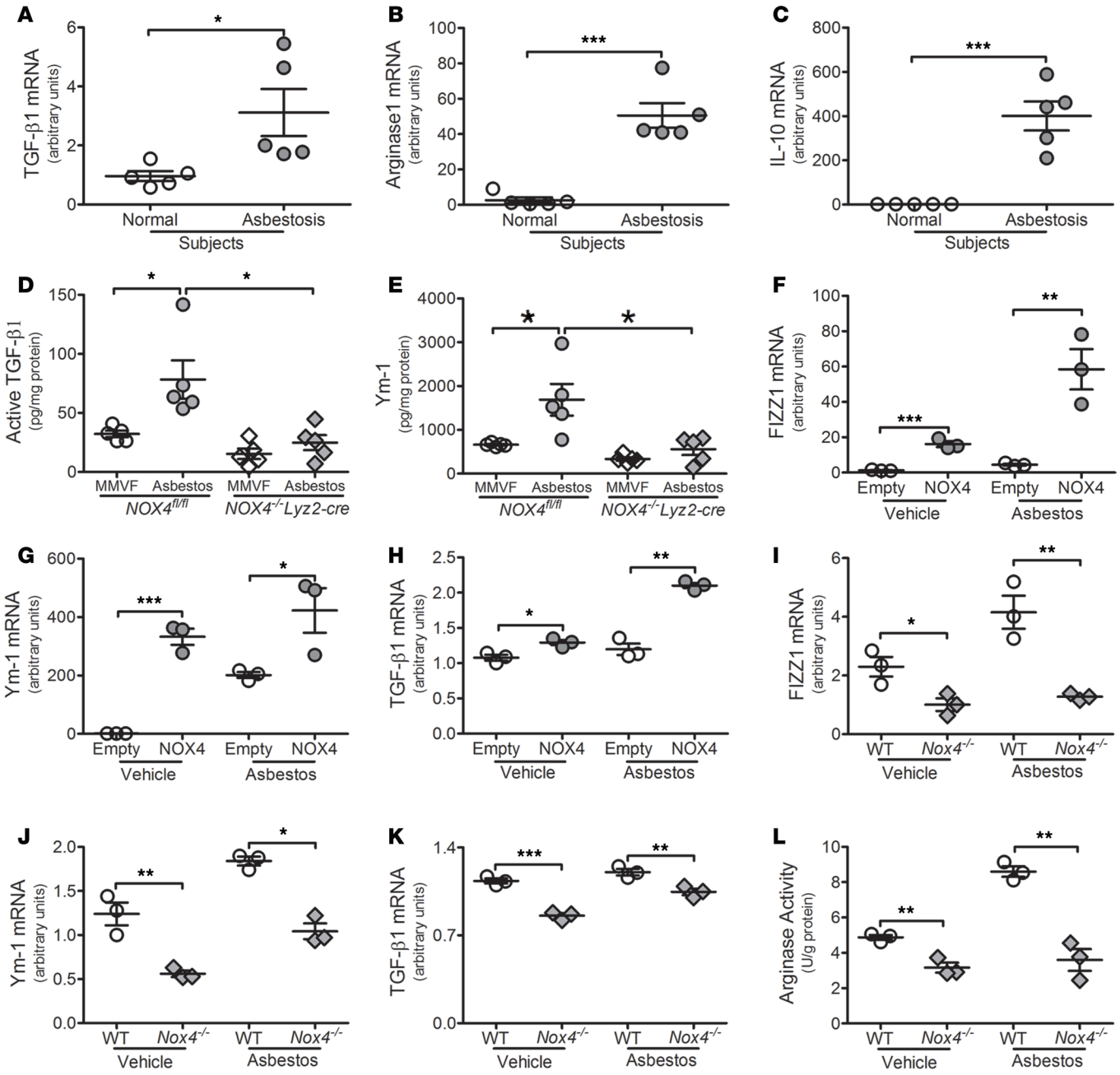

Figure 2. NOX4 regulates macrophage profibrotic polarization. mRNA expression in BAL cells from normal (n = 5) or asbestosis subjects (n = 5) for (**A**) TGF-β_1, (**B**) arginase 1, and (**C**) IL-10. (**D**) Active TGF-β_1 and (**E**) Ym-1 in BAL fluid (n = 5) from *Nox4*$^{fl/fl}$ and *Nox4*$^{-/-}$*Lyz2-Cre* mice exposed to either MMVF or chrysotile asbestos. (**F**) FIZZ1, (**G**) Ym-1, and (**H**) TGF-β_1 mRNA analysis of MH-S alveolar macrophages expressing empty vector or NOX4. (**I**) FIZZ1, (**J**) Ym-1, and (**K**) TGF-β_1 mRNA analysis of BMDMs from WT and *Nox4*$^{-/-}$ mice. (**L**) Arginase activity in BMDMs from WT and *Nox4*$^{-/-}$ mice. $^*P < 0.05$, $^{**}P < 0.01$, $^{***}P < 0.001$. Values shown as mean ± SEM. Two-tailed t test or 1-way ANOVA followed by Tukey's multiple-comparisons test was used. Each dot represents 1 human subject, 1 animal, or 1 sample. All in vitro experiments were repeated independently thrice, and representative blots are shown.

Several studies have shown an interdependence between mitochondrial biogenesis and mitophagy. We previously showed that mitophagy is elevated in profibrotic macrophages in bleomycin-induced fibrosis, and mitophagy is regulated by redox signals (12). Similarly, asbestos increased mitophagy in WT macrophages, whereas *Nox4*$^{-/-}$ macrophages had attenuated mitophagy in the presence or absence of asbestos (Supplemental Figure 3, J and K).

NOX4 augments mitochondrial ROS production. ROS are known to play a pivotal role in the development of pulmonary fibrosis. Lung macrophages are an important source of ROS production, and we have

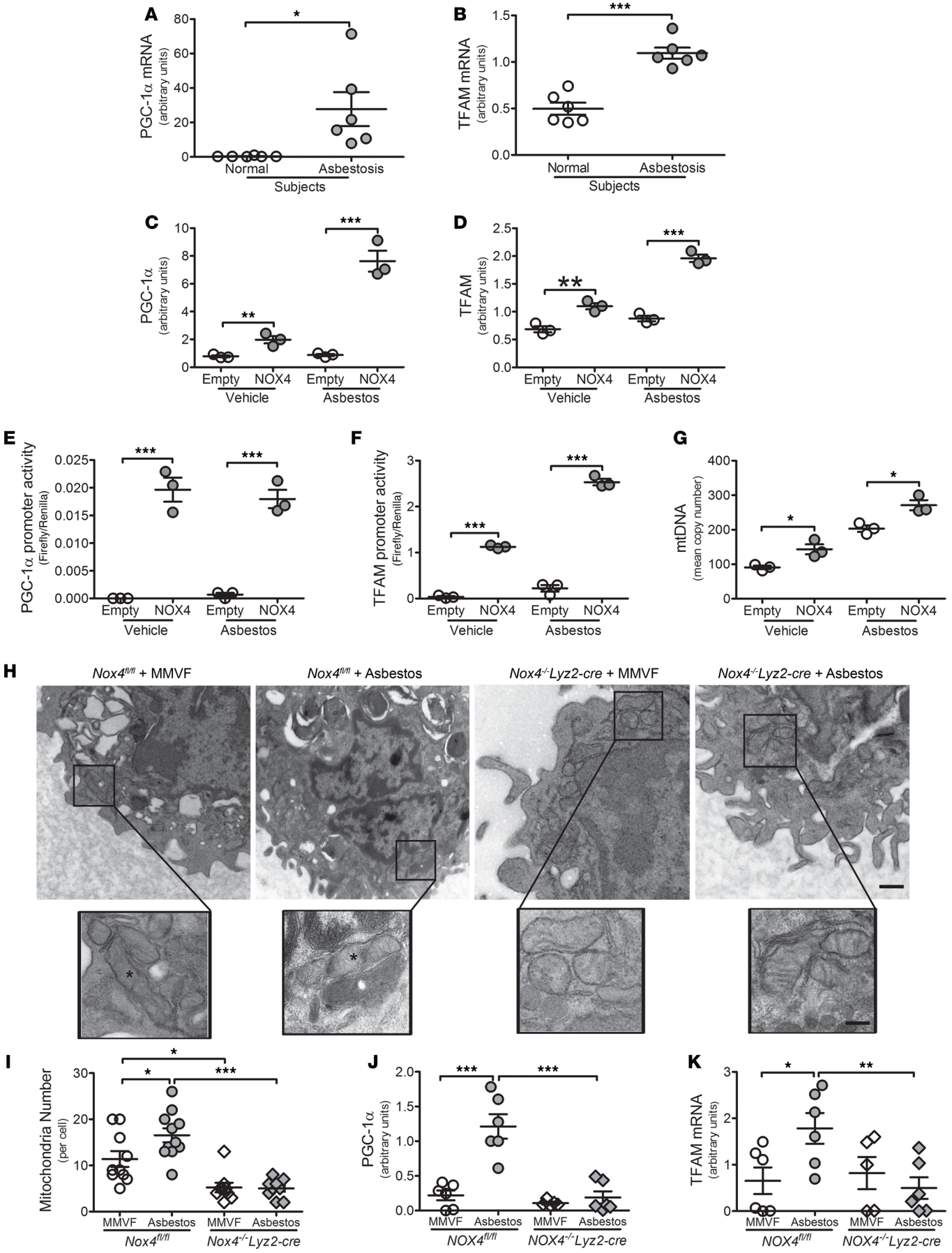
A
PGC-1α mRNA (arbitrary units)
Normal
Asbestosis
Subjects
B
TFAM mRNA (arbitrary units)
Normal
Asbestosis
Subjects
C
PGC-1α (arbitrary units)
Empty
NOX4
Vehicle
Asbestos
D
TFAM (arbitrary units)
E
PGC-1α promoter activity (Firefly/Renilla)
F
TFAM promoter activity (Firefly/Renilla)
G
mtDNA (mean copy number)
H
Nox4fl/fl + MMVF
Nox4fl/fl + Asbestos
Nox4-/-Lyz2-cre + MMVF
Nox4-/-Lyz2-cre + Asbestos
I
Mitochondria Number (per cell)
MMVF
Asbestos
Nox4fl/fl
Nox4-/-Lyz2-cre
J
PGC-1α (arbitrary units)
NOX4fl/fl
NOX4-/-Lyz2-cre
K
TFAM mRNA (arbitrary units)

Figure 3. NOX4 regulates mitochondrial biogenesis. (**A**) PGC-1α and (**B**) TFAM mRNA analysis of lung macrophages from normal (n = 6) or asbestosis subjects (n = 6). (**C**) PGC-1α and (**D**) TFAM mRNA analysis of MH-S lung macrophages expressing empty vector or NOX4 in the presence or absence of chrysotile asbestos. MH-S lung macrophages were transfected with (**E**) PGC-1α firefly luciferase vector or (**F**) TFAM firefly luciferase vector and either an empty or NOX4 vector. Firefly and *Renilla* luciferase activities were measured. Results are shown as firefly luciferase normalized to *Renilla* luciferase. (**G**) Mitochondrial DNA content in MH-S lung macrophages expressing empty vector or NOX4. (**H**) Transmission electron microscopy (TEM) analysis of lung macrophages from *Nox4*$^{fl/fl}$ and *Nox4*$^{-/-}$*Lyz2-Cre* mice exposed to either MMVF or chrysotile asbestos. Asterisk indicates elongated mitochondria. Scale bars: 500 nm (main), 100 nm (insets). (**I**) Total number of mitochondria per lung macrophage. (**J**) PGC-1α and (**K**) TFAM mRNA analysis of lung macrophages from *Nox4*$^{fl/fl}$ and *Nox4*$^{-/-}$*Lyz2-Cre* mice (n = 6) exposed to either MMVF or chrysotile asbestos. *P < 0.05, **P < 0.01, ***P < 0.001. Values shown as mean ± SEM. Two-tailed t test or 1-way ANOVA followed by Tukey's multiple-comparisons test was used. Each dot represents 1 human subject, 1 animal, or 1 sample. All in vitro experiments, including Western blotting, were repeated independently thrice, and representative blots are shown.

shown that mitochondrial ROS production is critical for profibrotic polarization (4, 5, 20); however, the mechanism by which this occurs is poorly understood. Lung macrophages from asbestosis subjects had increased mitochondrial H_2O_2 production (Figure 4A), and the rate of production was significantly greater than in normal subjects (Figure 4B). Asbestos-induced injury mediated 10-fold greater mitochondrial ROS production in *Nox4*$^{fl/fl}$ lung macrophages, whereas the ROS in the *Nox4*$^{-/-}$*Lyz2-Cre* mice were reduced to the MMVF control level (Figure 4C). Taken together, these data strongly suggest that NOX4, at least in part, contributes to mitochondrial ROS production.

Oxidative stress is known to reduce mitochondrial membrane potential. We asked whether NOX4-mediated ROS production altered mitochondrial membrane potential. There was increased green fluorescent JC-1 monomer in WT macrophages compared with *Nox4*$^{-/-}$ macrophages after asbestos exposure, indicating a relative reduction in membrane potential (Figure 4D). The ratio of green fluorescent JC-1 monomer to its red fluorescent aggregates was about 3-fold higher in WT macrophages compared with *Nox4*$^{-/-}$ macrophages (Figure 4E). These data suggest that NOX4-mediated mitochondrial ROS augmented asbestos-induced oxidative stress and reduced mitochondrial membrane potential.

Based on the regulation of mitochondrial ROS and membrane potential, we questioned whether mitochondrial bioenergetics was similarly regulated by NOX4. Lung macrophages from asbestos-injured WT mice had a significant increase in oxygen consumption compared with MMVF-treated WT mice, whereas the *Nox4*$^{-/-}$ macrophages had reduced oxygen consumption to the level of the WT control, regardless of asbestos exposure (Figure 4, F–H). Interestingly, the *Nox4*$^{-/-}$ macrophages had increased extracellular acidification rate (ECAR) compared with WT macrophages, suggesting a potential shift of metabolism toward glycolysis in the absence of NOX4 (Supplemental Figure 4A).

Mitochondrial ROS production alters the balance between different mitochondrial reducing and oxidizing equivalents, such as NADH and NAD^+ (21, 22). We measured NADH and NAD^+ in BMDMs from WT and *Nox4*$^{-/-}$ mice and found that *Nox4*$^{-/-}$ macrophages had an increased NADH/NAD^+ ratio (Supplemental Figure 4B). In contrast, the NADH/NAD^+ ratio was reduced in macrophages with NOX4 overexpression compared with those transfected with an empty vector (Supplemental Figure 4C). Moreover, asbestos exposure further reduced the NADH/NAD^+ ratio in macrophages overexpressing NOX4. Mitochondrial respiration and the NADH/NAD^+ ratio are closely related to mitochondrial ATP production. ATP production is known to be decreased in lung fibroblasts from pulmonary fibrosis subjects (23); however, the contribution of NOX4 in lung macrophages is not known. NOX4 deficiency in macrophages resulted in a marked decrease in ATP production (Supplemental Figure 4D). In aggregate, these data suggest that decreased mitochondrial biogenesis in *Nox4*$^{-/-}$ macrophages is associated with increased NADH reserve and reduced ATP production.

NOX4 mediates mitochondrial ROS production, which is pivotal for macrophage profibrotic phenotypic switching. Because NOX4 regulates mitochondrial ROS production and mitochondrial ROS production is known to regulate macrophage polarization (3–5), we questioned whether NOX4-mediated mitochondrial ROS production altered macrophage polarization. Mito-TEMPO treatment reduced mitochondrial NOX4 expression, suggesting NOX4 expression is redox regulated (Supplemental Figure 5A). Mito-TEMPO reduced mitochondrial H_2O_2 production in WT macrophages to the level in vehicle-treated *Nox4*$^{-/-}$ macrophages (Figure 5, A and B). To test whether Mito-TEMPO treatment regulated mitochondrial biogenesis, we measured the expression of *pgc1a*. Mito-TEMPO significantly reduced *pgc1a* expression, regardless of whether NOX4 was overexpressed (Figure 5C). Accompanied with the reduced level of *pgc1a*, we found Mito-TEMPO treatment reduced arginase activity (Figure 5D) and active TGF-β_1 production (Figure 5E) in WT macrophages to a level similar to *Nox4*$^{-/-}$ macrophages. These data suggest the NOX4 expression augments mitochondrial ROS production. Furthermore, abrogating NOX4-derived mitochondrial ROS reduced mitochondrial biogenesis

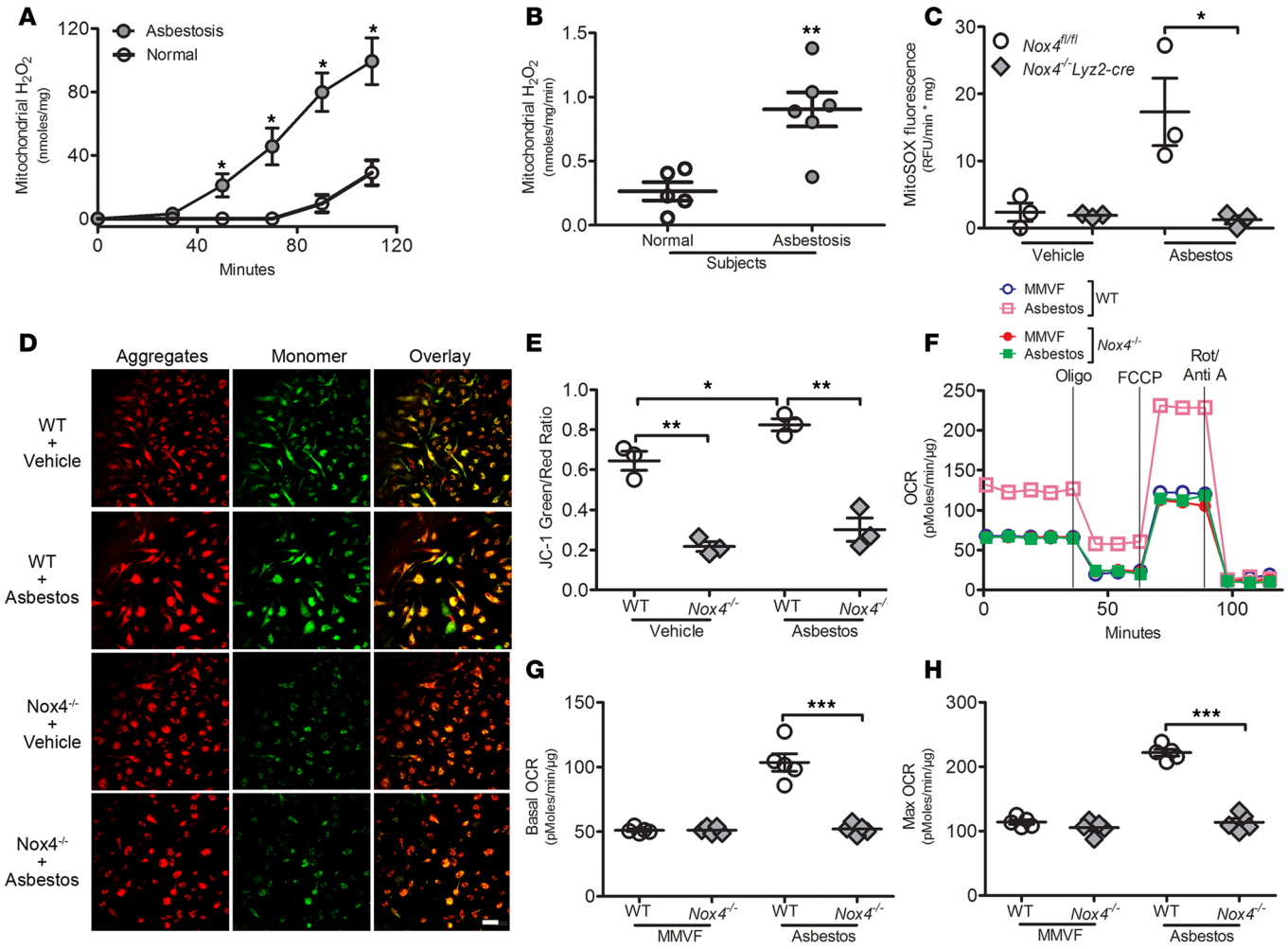

Figure 4. NOX4 regulates mitochondrial ROS and bioenergetics. (**A** and **B**) H_2O_2 generation in isolated mitochondria of lung macrophages from normal (n = 5) or asbestosis subjects (n = 6). (**C**) ROS production of lung macrophages from *Nox4*$^{fl/fl}$ and *Nox4*$^{-/-}$*Lyz2-Cre* mice (n = 3) exposed to either MMVF or chrysotile asbestos measured by MitoSOX. (**D**) Mitochondrial membrane potential measured in BMDMs from WT and *Nox4*$^{-/-}$ mice by JC-1. Red, JC-1 aggregates; green, JC-1 monomer; overlay, JC-1 red and green fluorescent overlay. (**E**) Quantification of JC-1 green/red fluorescence ratio (n = 3). (**F**) Oxygen consumption rate (OCR) tracing, (**G**) basal OCR, and (**H**) maximal OCR of lung macrophages from WT and *Nox4*$^{-/-}$ mice exposed to either MMVF or chrysotile asbestos (n = 5). $^*P < 0.05$, $^{**}P < 0.01$, $^{***}P < 0.001$. Values shown as mean ± SEM. Two-tailed t test or 1-way ANOVA followed by Tukey's multiple-comparisons test was used. Each dot represents 1 human subject, 1 animal, or 1 sample. All in vitro experiments, including Western blotting, were repeated independently thrice, and representative blots are shown.

and profibrotic polarization. Mito-TEMPO decreased ATP production in WT macrophages (Supplemental Figure 5B), again indicating the relevance of NOX4-derived ROS in macrophages during fibrotic repair.

Lung macrophage profibrotic polarization is regulated via modulation of mitochondrial biogenesis. Because mitochondrial biogenesis is elevated in lung macrophages from fibrotic subjects and mice, and those macrophages maintain a profibrotic phenotype, we asked whether the macrophage phenotype was dependent on mitochondrial biogenesis. Silencing PGC-1α significantly reduced *tfam* expression, validating the requirement of PGC-1α for biogenesis (Figure 6A). NOX4 increased *fizz1*, and silencing PGC-1α significantly decreased *fizz1* gene expression (Figure 6B). NOX4 overexpression was unable to rescue *fizz1* gene expression in PGC-1α–deficient macrophages, suggesting that PGC-1α is required for NOX4-mediated profibrotic polarization. Similarly, silencing PGC-1α reduced arginase activity (Supplemental Figure 6A) and active TGF-β_1 production (Figure 6C). Additionally, silencing PGC-1α increased NADH/NAD$^+$ ratio (Supplemental Figure 6B). This change in NADH/NAD$^+$ ratio was sustained even in the setting of NOX4 overexpression. Taken together, these data emphasize the importance of PGC-1α, a critical regulator of mitochondrial biogenesis, in the process of NOX4-mediated macrophage polarization. Modulating mitochondrial biogenesis can effectively attenuate the macrophage phenotypic switching to profibrotic activation.

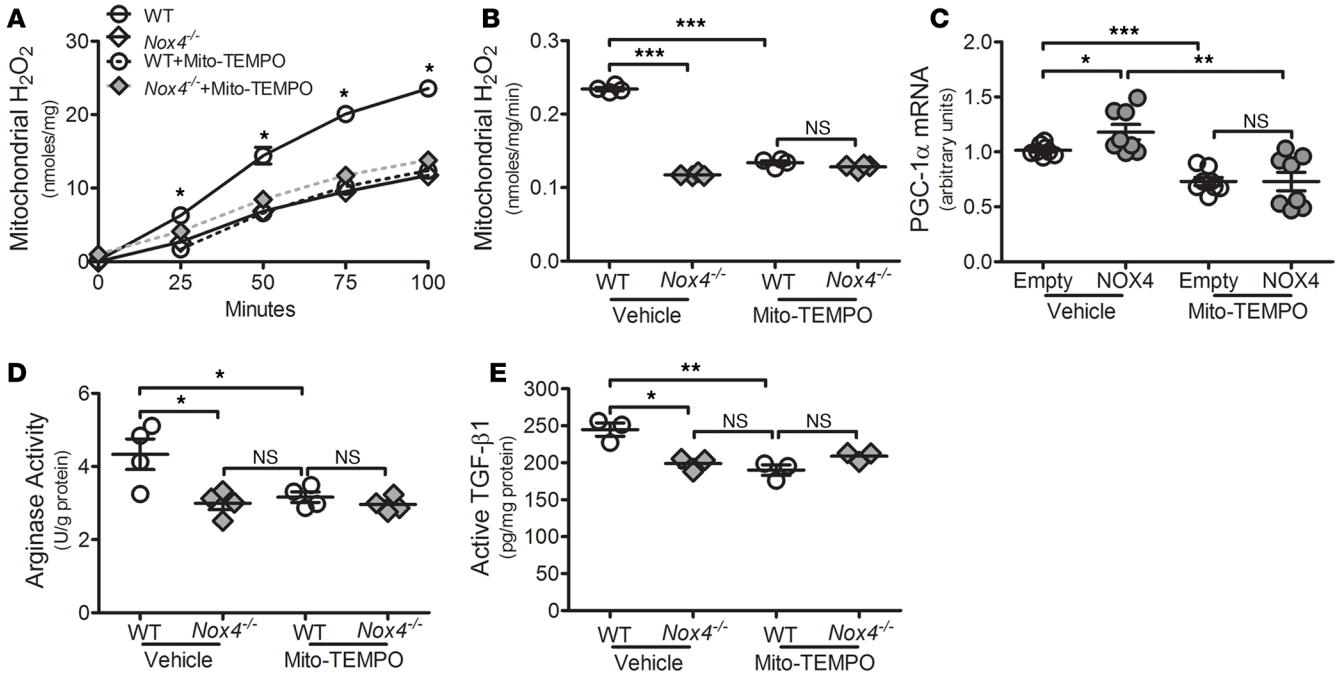

Figure 5. Modulation of mitochondrial ROS regulates profibrotic polarization. (**A** and **B**) H_2O_2 generation in isolated mitochondria of BMDMs from WT and *Nox4*$^{-/-}$ mice in the presence or absence of Mito-TEMPO. (**C**) PGC-1α mRNA analysis in MH-S lung macrophages expressing either an empty or NOX4 vector in the presence or absence of Mito-TEMPO. (**D**) Arginase activity in BMDMs from WT and *Nox4*$^{-/-}$ mice in the presence or absence of Mito-TEMPO. (**E**) Active TGF-β_1 in conditioned medium of BMDMs from WT and *Nox4*$^{-/-}$ mice in the presence or absence of Mito-TEMPO. **P* < 0.05, ***P* < 0.01, ****P* < 0.001. Values shown as mean ± SEM. Two-tailed *t* test or 1-way ANOVA followed by Tukey's multiple-comparisons test was used. Each dot represents 1 human subject, 1 animal, or 1 sample. All in vitro experiments were repeated independently thrice, and representative blots are shown.

Fusion, fission, and division are mechanisms for mitochondrial biogenesis (24). Mdivi-1, a chemical compound that selectively inhibits dynamin-related GTPase (Drp-1), has been investigated in preclinical trials for neurodegenerative disease, myocardial infarction, and cancer (25–27); however, the involvement of Drp-1 in fibrotic repair is not known. Phosphorylated Drp-1 was significantly greater in mitochondria from subjects with asbestosis compared with those from normal subjects (Figure 6D). These data suggest that mitochondrial biogenesis occurs by fission rather than fusion because Mfn-2 was decreased in lung macrophages from subjects with asbestosis (data not shown). This was supported by showing that Mdivi-1 decreased PGC-1α expression significantly to the level in the vehicle-treated macrophages (Figure 6E), suggesting that Mdivi-1 can inhibit mitochondrial biogenesis.

Given its inhibitory effects on mitochondrial biogenesis in macrophages, we further investigated whether Mdivi-1 can also prevent macrophage profibrotic activation and reduce the production of profibrotic molecules. Macrophages treated with Mdivi-1 had reduced *tgfb1* promoter activity compared with vehicle-treated macrophages (Figure 6F). In macrophages overexpressing NOX4, Mdivi-1 reduced *tgfb1* promoter activity to one-third of the level seen in the vehicle-treated macrophages. Mdivi-1 also decreased active TGF-β_1 production in WT and *Nox4*$^{-/-}$ BMDMs (Figure 6G). Moreover, Mdivi-1 can block active TGF-β_1 production in macrophages even after asbestos exposure, providing a promising approach to abrogating TGF-β_1 production and fibrosis progression.

NOX4 was recently found to bind 2 subunits within mitochondrial complex I and reduced mitochondrial complex I protein expression in human endothelial cells (28, 29). We found similar expression of mitochondrial complex I in WT and *Nox4*$^{-/-}$ macrophages (Supplemental Figure 6C). Additionally, overexpression of NOX4 did not alter complex I activity (Supplemental Figure 6D). Mdivi-1, in addition of its function as Drp-1 inhibitor, was recently found to inhibit mitochondrial complex I activity and reduced mitochondrial H_2O_2 production in isolated brain mitochondria (30). We found that Mdivi-1 treatment does not change mitochondrial complex I activity in macrophages (Supplemental Figure 6E). Collectively, these data demonstrate a critical role of mitochondrial biogenesis in macrophage polarization and provide what we believe to be novel perspectives in targeting macrophage NOX4 in asbestos-induced pulmonary fibrosis.

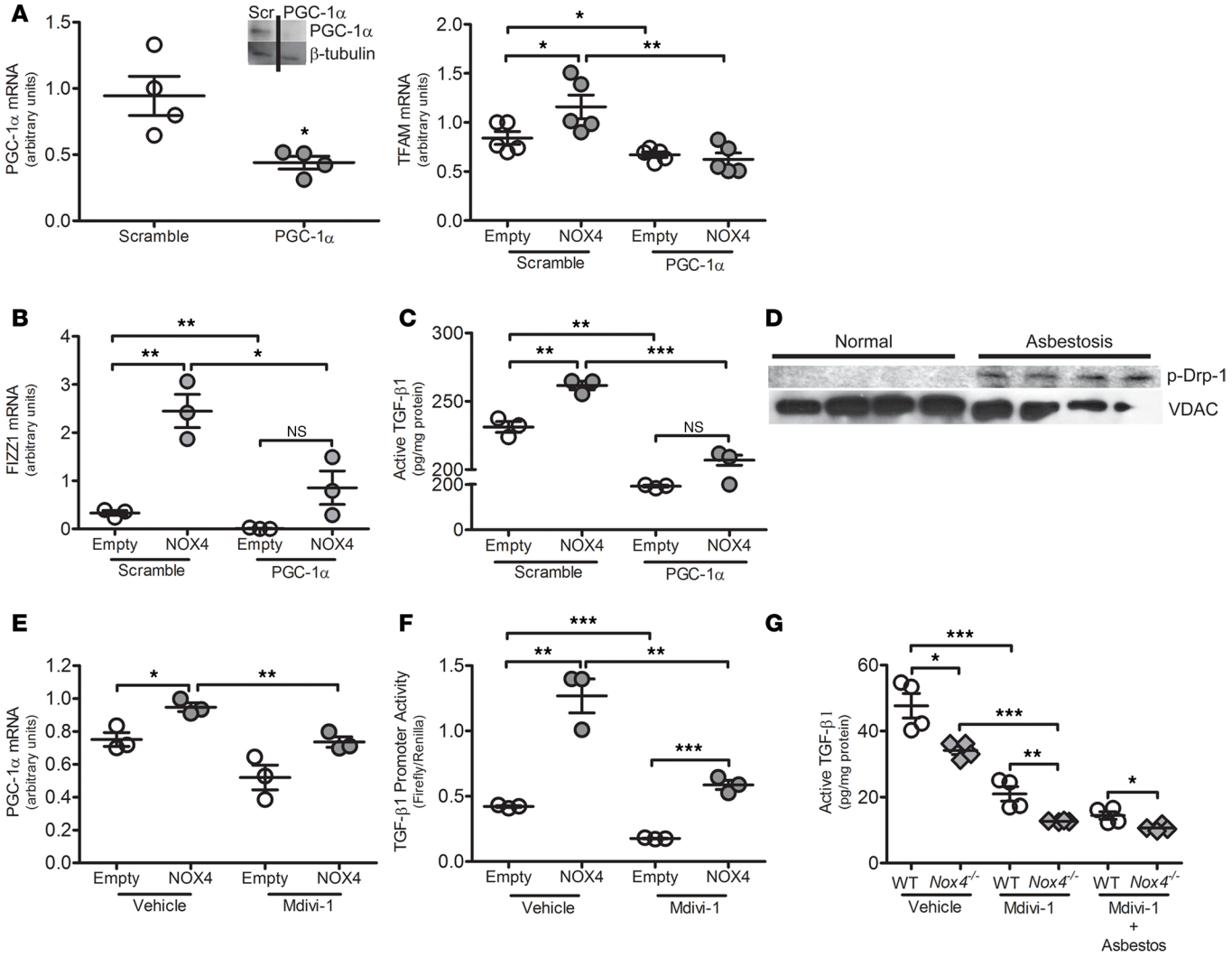

Figure 6. Modulation of mitochondrial biogenesis programs profibrotic polarization. (**A**) PGC-1α mRNA analysis in MH-S lung macrophages transfected with either scrambled or PGC-1α siRNA. Inset, immunoblot of PGC-1α in MH-S lung macrophages transfected with either scrambled or PGC-1α siRNA. TFAM mRNA analysis in MH-S lung macrophages transfected with either scrambled or PGC-1α siRNA with empty or NOX4 vector. (**B**) FIZZ1 mRNA analysis in MH-S lung macrophages transfected with either scrambled or PGC-1α siRNA with empty or NOX4 vector. (**C**) Active TGF-β_1 in conditioned medium of MH-S lung macrophages transfected with either scrambled or PGC-1α siRNA with empty or NOX4 vector. (**D**) Immunoblot of phosphorylated Drp-1 (p–Drp-1) in mitochondria of lung macrophages from normal (n = 4) or asbestosis subjects (n = 4). (**E**) PGC-1α mRNA analysis in MH-S lung macrophages expressing empty or NOX4 vector in the presence or absence of Mdivi-1 (20 μM). (**F**) TGF-β_1 firefly luciferase activity in MH-S lung macrophages expressing empty or NOX4 vector in the presence or absence of Mdivi-1 (20 μM). Results are shown as firefly luciferase normalized to *Renilla* luciferase. (**G**) Active TGF-β_1 in conditioned medium of BMDMs from WT and *Nox4*$^{-/-}$ mice in the presence or absence of Mdivi-1 and chrysotile asbestos. *P < 0.05, **P < 0.01, ***P < 0.001. Values shown as mean ± SEM. Two-tailed t test or 1-way ANOVA followed by Tukey's multiple-comparisons test was used. Each dot represents 1 human subject, 1 animal, or 1 sample. All in vitro experiments, including Western blotting, were repeated independently thrice, and representative blots are shown.

Discussion

Pulmonary fibrosis is a disease condition generally considered irreversible and has a high mortality (31). NOX4 has been shown to be increased in myofibroblasts from subjects with idiopathic pulmonary fibrosis, and NOX4-mediated H_2O_2 production is required during myofibroblast differentiation and collagen synthesis (9). Silencing NOX4 in myofibroblasts has been shown to attenuate pulmonary fibrosis; however, the role of NOX4 in lung macrophages has not been examined. Our data suggest that NOX4 is greater in lung macrophages from subjects with asbestosis and is associated with increased mitochondrial ROS production. Furthermore, deletion of NOX4, specifically in lung macrophages, abrogated asbestos-induced fibrosis.

Lung macrophages are an important source of ROS during pulmonary fibrosis. It is known that macrophage NOX4 expression is increased in conditions characterized by increased oxidative stress, such as atherosclerosis, diabetes, and chronic alcohol abuse (32–34). Targeting NOX4 in monocytes/

macrophages and reducing NOX4-mediated ROS production is known to be protective in several disease conditions, such as cardiac ischemia/reperfusion injuries, diabetes, and *Streptococcus pneumoniae* infection (8, 35, 36). Here, we show that NOX4-derived ROS are critical for profibrotic cytokine production, and reducing ROS production by deleting NOX4 in macrophages can decrease profibrotic polarization. Recent studies suggest that there are many potential contacts between NOX4 and critical mitochondrial components (28, 29, 37). In addition to the proposed interaction between NOX4 and mitochondrial complex I subunits previously described, ATP can directly bind to NOX4 and negatively regulate its activity in normal renal epithelial cells and renal carcinoma cells (37); however, our data demonstrate that ATP production is NOX4 dependent.

Macrophages are highly plastic and will program into different phenotypes in various disease conditions. Profibrotic macrophages increase the generation of profibrotic cytokines and provide substrate for collagen synthesis. Targeting this macrophage phenotype has been examined in several preclinical studies to reduce or prevent pulmonary fibrosis (3–5, 38–40). A prior study showed that NOX4 was decreased in iPLA2β$^{-/-}$ macrophages, which harbor a profibrotic phenotype (41). We are the first to our knowledge to show that NOX4 mediates macrophage polarization to a profibrotic phenotype, as we observed in human subjects with lung fibrosis and in our murine model.

Recent advances in the field have highlighted the key role of MDMs in promoting fibrosis (15, 42), and increasing circulating monocyte counts have been shown to be a poor prognostic indicator in pulmonary fibrosis (43). Our data support the notion that MDMs are crucial in aberrant repair because there are increased numbers of MDMs in the lungs of mice developing fibrosis. Although the mechanism of the recruitment was not determined here, several studies have shown monocyte chemoattractant protein 1 production from AECII is responsible for the increase in monocytic cells in BAL after injury (44, 45); however, the mechanism of recruitment in asbestos-induced injury warrants further investigation.

Fluctuations in mitochondrial function are a universal phenomenon among different fibrotic lung diseases. Removal of dysfunctional mitochondria by mitophagy and generating new mitochondria by biogenesis are 2 regulatory mechanisms to keep a homeostatic pool of mitochondria. Unbalanced changes in either pathway will cause disruption in mitochondrial homeostasis. We previously showed that mitophagy is increased in lung macrophages from subjects with idiopathic pulmonary fibrosis and bleomycin-injured mice (12). Previous data showed that NOX4 suppressed mitochondrial biogenesis in lung fibroblasts in vitro (17), as well as reduced biogenesis in response to a fibrotic injury in vivo (13). Another study showed that mitochondrial biogenesis was also decreased in alveolar epithelial cells from mice after bleomycin injury (14). Our data reveal that NOX4 regulated mitochondrial dynamics in a different manner. Mitochondrial biogenesis was increased in lung macrophages from subjects with fibrotic lung disease and in asbestos-injured mice. In concordance with other studies that showed a central role of PGC-1α in mitochondrial biogenesis, our study also showed that NOX4 regulates PGC-1α, and PGC-1α is required for NOX4-mediated mitochondrial biogenesis.

The observed increase in mitochondrial biogenesis appears to be critical for sustaining the profibrotic phenotype of macrophages. Macrophages deficient in either CR6-interacting factor 1 or growth differentiation factor 15 have a predominantly proinflammatory phenotype and are unable to polarize into the alternatively activated phenotype (46, 47). Mitochondrial biogenesis was significantly reduced with a deficiency of either factor. Mitochondrial oxidative phosphorylation (OXPHOS) is known to be altered during certain macrophage polarization programs. Specifically, a sustained high level of OXPHOS is required to maintain a profibrotic phenotype, whereas IFN-γ treatment will dampen OXPHOS and polarize macrophage toward the proinflammatory phenotype (48). In a colitis animal model, mitochondrial ROS are crucial for the alternative activation of macrophages, and a reduction in mitochondrial ROS using the mitochondria-targeted antioxidant MitoQ reduced the number of alternatively activated macrophages (49). Our observations indicated that *Nox4*$^{-/-}$ macrophages failed to polarize to the profibrotic phenotype, had reduced mitochondrial ROS production, and had decreased ATP production, supporting the concept that mitochondrial ROS, OXPHOS, and biogenesis are critical for the maintenance of the profibrotic macrophage phenotype, which is critical for fibrotic repair after asbestos exposure.

Methods

Human subjects. Normal volunteers (male and female) had to meet the following criteria: (a) age between 25 and 75 years, (b) no history of cardiopulmonary disease or other chronic disease, (c) no prescription or nonprescription medication except oral contraceptives, (d) no recent or current evidence of infection, and

(e) lifetime nonsmoker. Subjects with asbestosis (male predominant) had to meet the following criteria: (a) evidence of restrictive physiology on pulmonary function tests, (b) forced vital capacity greater than 50%, (c) current nonsmoker, (d) no recent or current evidence of infection, (e) usual interstitial pneumonia on chest high-resolution computed tomography, and (f) strong history of asbestos exposure or presence of pleural plaque on chest high-resolution computed tomography. The percentage of macrophages was determined by Wright-Giemsa stain and varied from 90% to 98%.

Mice. *Nox4*$^{-/-}$*Lyz2-Cre* mice were generated by selective disruption of *Nox4* gene in the cells of the granulocyte/monocyte lineage by crossing *Nox4*$^{fl/fl}$ mice with mice containing a Cre recombinase under the control of the lysozyme M promoter. The *Nox4*$^{-/-}$ mice have been previously described (10). Mice were intratracheally administered 100 μg of chrysotile asbestos suspended in 50 μL 0.9% saline solution after being anesthetized with 3% isoflurane using a precision Fortec vaporizer (Cyprane). Mice were euthanized at the designated day after exposure with an overdose of isoflurane, and BAL was performed. Bone marrow cells were isolated and incubated in L929 cell–conditioned medium (generated in-house) for 7 days to generate macrophages. The lungs were removed and stained for collagen fibers using Masson's trichrome stain.

Cell culture. Mouse alveolar macrophage (MH-S) cell lines were obtained from ATCC. Cells were maintained in RPMI-1640 medium (Thermo Fisher Scientific) with the following supplements: 10% fetal bovine serum and penicillin/streptomycin. All experiments were performed with 0.5% serum supplement.

Plasmids and transfections. Human NOX4 cDNA was subcloned into pcDNA3.1 between the KpnI (5′) and NotI (3′) sites. Plasmid vectors were transfected into cells using X-tremeGene 9 transfection reagent (Roche), according to the manufacturer's instructions.

Quantitative real-time PCR. Total RNA was obtained using Trizol reagent (MilliporeSigma). After we performed reverse transcription using iScript reverse transcription kit (Bio-Rad Laboratories), specific gene mRNA expression was determined by quantitative real-time PCR using the SYBR Green kit (Bio-Rad Laboratories). The following primer sets were used, although mouse Ym1, mouse FIZZ1, mouse β-actin, mouse TGF-β_1, and human HPRT have been previously described (50): human NOX4, 5′-CGTCTGGGCAGCTGAGTG-3′ and 5′-GAGCCAGATGAACAGGCAGA-3′; human PGC-1α, 5′-GAGTGTGTGCTCTGTGTCACT-3′ and 5′-CAGCACACTCGATGTCACTCCAT-3′; human TFAM, 5′-GAACAACTACCCATATTTAAAGCTCA-3′ and 5′-GAATCAGGAAGTTCCCTCCA-3′; mouse citrate synthase, 5′-CTGCTCCAGTACTATGGCATGA-3′ and 5′-TTAAAGGCCCCTGAAACAAAACA-3; mouse COX IV, 5′-CCGTCTTGGTCTTCCGGTTG-3′ and 5′-TGGAAGCCAACATTCTGCCA-3′; mouse Drp-1, 5′-GCCTCAGATCGTCGTAGTGG-3′ and 5′-TGCTTCAACTCCATTTTCTTCTCC-3′; mouse PGC-1α, 5′-GGCAGTAGATCCTCTTCAAGATC-3′ and 5′-TCACACGGCGCTCTTCAATTG-3′; and mouse TFAM, 5′-CCAAAAAGACCTCGTTCAGC-3′ and 5′-CCATCTGCTCTTCCCAAGAC-3′. Data were calculated by the ΔΔCT method. The mRNA measurements were normalized to β-actin or HPRT and expressed in arbitrary units.

Isolation of nucleus, cytoplasm, mitochondria, and mitoplasts. Cellular compartment separation was performed as described previously (5, 20).

Luciferase assays. PGC-1α gene expression was evaluated using a luciferase reporter plasmid purchased from Addgene, plasmid 8887. TFAM luciferase reporter plasmid was a gift from David Hood (York University, Toronto, Ontario, Canada). *Renilla* and firefly luciferase activities were determined in cell lysates using the Dual Luciferase reporter assay kit (Promega).

TEM. TEM was performed as previously described (12). Macrophages were fixed in 2.5% paraformaldehyde and 2.5% glutaraldehyde in Sorenson's phosphate buffer (Electron Microscopy Science) at pH 7.4. After fixation, cells were processed and sectioned with a diamond knife (Diatome, Electron Microscopy Sciences) at 70–80 nm, and sections were placed on copper mesh grids (Electron Microscopy Science). Sections were stained with the heavy metals uranyl acetate and lead citrate for contrast and viewed on a Tecnai Twin 120kv TEM (FEI).

Quantification of mtDNA. The ratio of mitochondrial to nuclear DNA was assessed using the Human Mitochondrial DNA Monitoring Primer Set Ratio kit (Takara Bio).

Determination of ROS generation. H_2O_2 production was determined fluorometrically, as previously described (51). ROS were also measured in live cells using dihydroethidium derivative (MitoSOX; Thermo Fisher Science) at 5 μM. After incubation, cells were washed twice. Fluorescence was measured using a SpectraMax M2 plate reader (Molecular Devices).

Measurement of mitochondrial membrane potential. Cells were loaded with JC-1 dye (Molecular Probes) at a final concentration of 10 μg/mL for 15 minutes at 37°C. Cells were imaged using Zeiss LSM 710 confocal microscope, and all images were taken at the same time using the same imaging settings.

OCR and ECAR determination. OCR and ECAR were determined using a Seahorse XF24 bioanalyzer (Seahorse Bioscience) as previously described (4, 52).

NADH and NAD$^+$ measurement. The measurement was performed with the Fluorimetric NADH/NAD$^+$ Ratio Assay Kit (AAT Bioquest 15263), based on the manufacturer's instructions.

Mitochondrial ATP measurement. Mitochondrial ATP was quantitated by CellTiter-Glo Luminescent Cell Viability Assay kit (Promega) as previously described (4), according to the manufacturer's instructions.

Arginase activity assay. Arginase activity was measured by using a QuantiChrom Arginase Assay Kit (BioAssay System), according to manufacturer's instructions.

siRNA. Cells were transfected with 100 nM scrambled or PGC-1α siRNA duplex (IDT) using DharmaFect 4 reagent (Dharmacon Research) as previously described (53).

Hydroxyproline determination. Lung tissue was dried and digested for 24 hours at 112°C with 6N hydrochloric acid. Hydroxyproline concentration was determined as previously described (5).

Indirect immunofluorescence assay. Cells were fixed with 4% formaldehyde at room temperature for 45 minutes, followed by permeabilization for 3 minutes in ice-cold buffer (0.1% sodium citrate and 0.1% Triton X-100 in distilled water). Cells were then blocked at room temperature for 1 hour in DPBS with 1% BSA. Cells were incubated with NOX4 Ab (Abcam, catalog ab109225), FITC-conjugated mouse anti-rabbit Ab (SouthernBiotech, catalog 4030-02), MitoTracker Red (Thermo Fisher Scientific), and DAPI. All images of specific interests were quantitated using ImageJ (NIH).

Immunoblot analysis. NOX4 rabbit Abs (Abcam, ab154244; Abcam, ab133303; Novus Biologicals, NB110-58849), TFAM rabbit Ab (Cell Signaling Technology, 8076), PGC-1α rabbit Ab (MilliporeSigma, AB3242), VDAC rabbit Ab (Cell Signaling Technology, 4866), p–Drp-1 (S616) rabbit Ab (Cell Signaling Technology, 3455), β-actin mouse Ab (MilliporeSigma, A5441), LC-3 rabbit Ab (Cell Signaling Technology, 4108), rodent total OXPHOS Ab (Abcam, ab110413), Parkin rabbit Ab (Cell Signaling Technology, 2132S), p–p38 MAPK rabbit Ab (Cell Signaling Technology, 9215S), p38 (H-147) rabbit Ab (Santa Cruz Biotechnology, sc-7149), and SOD1 sheep Ab (MilliporeSigma, 07-403-I) were used for immunoblot analysis. Densitometry was determined using ImageJ.

Flow cytometry. BAL cells were blocked with 1% BSA containing TruStain fcX (anti–mouse CD16/32) Ab (BioLegend, 101319), followed by staining with Abs. Abs used were rat anti–mouse CD45-PE (eBiosciences, 12-0451-82), LIVE Dead eFluor 506 (Invitrogen, 65-0866), rat anti–mouse CD11b-APC-Cy7 (BioLegend, 101225), anti–mouse CD64-PE-Cy7 (BioLegend, 139313), rat anti–mouse Ly6G-AF700 (BD, 561236), rat anti–mouse Siglec FAPC (BioLegend, 155507), rat anti–mouse Ly6C: eFluor 450 (Invitrogen, 48-5932-82), Armenian hamster anti–mouse CD11c-FITC (BioLegend, 117305), and rat anti–mouse MHC II PerCP-Cy5.5 (BD, 562363). Hierarchical gating strategy was used to represent the resident alveolar macrophages as CD45$^+$CD11b$^{+/-}$Ly6G$^-$CD64$^+$Ly6c$^-$SiglecF^{hi} and MDMs as CD45$^+$CD11b$^{+/-}$Ly6G$^-$CD64$^+$Ly6c$^-$SiglecF^{lo}. Data were acquired on an LSR II (BD Biosciences) using BD FACSDIVA software (version 8.0.1). Data were analyzed using FlowJo (FlowJo LLC) software (version 10.5.0).

ELISA. Active TGF-β and Ym-1 levels in BAL fluid and cell media were measured by ELISA (R&D Systems), according to the manufacturer's instructions.

Complex I activity. Complex I activity was measured as previously described (54). Briefly, isolated mitochondria were intubated in solution containing 2,6-dichlorophenolindophenol (DCIP), decylubiquinone, and NADH. Complex I activity was expressed as rate of DCIP reduction.

Statistics. Statistical comparisons were performed as indicated in the figure legends and include the 2-tailed *t* test or 1-way ANOVA followed by Tukey's multiple-comparisons test. Values in figures are expressed as means ± SEM, and *P* value less than 0.05 was considered significant.

Study approval. We obtained human lung macrophages, as previously described (20), from normal and asbestosis subjects under an approved protocol (no. 300001124) by the Human Subjects Review Board of the University of Alabama at Birmingham. All patients provided prior written consent to participate in the study.

All animal protocols were approved (protocol 21149) by the University of Alabama at Birmingham Institutional Animal Care and Use Committee.

Author contributions

CH and ABC developed the concept and design of the study. CH, JLLC, LG, VSH, ALFL, DD, and ABC assisted with conducting experiments. CH, JLLC, LG, VSH, ALFL, and ABC acquired data. CH, JLLC, LG, VJT, and ABC provided reagents. CH, JLLC, LG, VSH, ALFL, VJT, and ABC provided analysis and interpretation of experiments and results. CH and ABC wrote the manuscript.

Acknowledgments

NIH grants R01ES015981-11 and 1R56ES027464-01 (to ABC) and 5T32HL105346 (to VJT and CH) and a Merit Review from the Department of Veterans Affairs, Veterans Health Administration, Office of Research and Development, Biomedical Laboratory Research and Development I01CX001715 (to ABC) supported this work. Support for the Comprehensive Flow Cytometry Core was provided by NIH P30AR048311 and NIH P30AI27667. The authors thank Edward Philips and Melissa Foley-Chimento and the University of Alabama at Birmingham High Resolution Imaging Facility for assistance with TEM.

Address correspondence to: A. Brent Carter, 1918 University Blvd., 404 MCLM, Pulmonary, Allergy, and Critical Care Medicine, University of Alabama at Birmingham, Birmingham, Alabama 35294, USA. Phone: 205.996.1682; Email: bcarter1@uab.edu.

1. Wynn TA, Vannella KM. Macrophages in tissue repair, regeneration, and fibrosis. *Immunity*. 2016;44(3):450–462.
2. Schumacker PT, et al. Mitochondria in lung biology and pathology: more than just a powerhouse. *Am J Physiol Lung Cell Mol Physiol*. 2014;306(11):L962–L974.
3. He C, Ryan AJ, Murthy S, Carter AB. Accelerated development of pulmonary fibrosis via Cu,Zn-superoxide dismutase-induced alternative activation of macrophages. *J Biol Chem*. 2013;288(28):20745–20757.
4. Gu L, Larson-Casey JL, Carter AB. Macrophages utilize the mitochondrial calcium uniporter for profibrotic polarization. *FASEB J*. 2017;31(7):3072–3083.
5. He C, Larson-Casey JL, Gu L, Ryan AJ, Murthy S, Carter AB. Cu,Zn-superoxide dismutase-mediated redox regulation of Jumonji domain containing 3 modulates macrophage polarization and pulmonary fibrosis. *Am J Respir Cell Mol Biol*. 2016;55(1):58–71.
6. Bedard K, Krause KH. The NOX family of ROS-generating NADPH oxidases: physiology and pathophysiology. *Physiol Rev*. 2007;87(1):245–313.
7. Block K, Gorin Y, Abboud HE. Subcellular localization of Nox4 and regulation in diabetes. *Proc Natl Acad Sci USA*. 2009;106(34):14385–14390.
8. Moon JS, et al. NOX4-dependent fatty acid oxidation promotes NLRP3 inflammasome activation in macrophages. *Nat Med*. 2016;22(9):1002–1012.
9. Hecker L, et al. NADPH oxidase-4 mediates myofibroblast activation and fibrogenic responses to lung injury. *Nat Med*. 2009;15(9):1077–1081.
10. Carnesecchi S, et al. A key role for NOX4 in epithelial cell death during development of lung fibrosis. *Antioxid Redox Signal*. 2011;15(3):607–619.
11. Mora AL, Bueno M, Rojas M. Mitochondria in the spotlight of aging and idiopathic pulmonary fibrosis. *J Clin Invest*. 2017;127(2):405–414.
12. Larson-Casey JL, Deshane JS, Ryan AJ, Thannickal VJ, Carter AB. Macrophage Akt1 kinase-mediated mitophagy modulates apoptosis resistance and pulmonary fibrosis. *Immunity*. 2016;44(3):582–596.
13. Rangarajan S, et al. Metformin reverses established lung fibrosis in a bleomycin model. *Nat Med*. 2018;24(8):1121–1127.
14. Yu G, et al. Thyroid hormone inhibits lung fibrosis in mice by improving epithelial mitochondrial function. *Nat Med*. 2018;24(1):39–49.
15. Misharin AV, et al. Monocyte-derived alveolar macrophages drive lung fibrosis and persist in the lung over the life span. *J Exp Med*. 2017;214(8):2387–2404.
16. Kuroda J, Ago T, Matsushima S, Zhai P, Schneider MD, Sadoshima J. NADPH oxidase 4 (Nox4) is a major source of oxidative stress in the failing heart. *Proc Natl Acad Sci USA*. 2010;107(35):15565–15570.
17. Scarpulla RC. Metabolic control of mitochondrial biogenesis through the PGC-1 family regulatory network. *Biochim Biophys Acta*. 2011;1813(7):1269–1278.
18. Fernandez-Marcos PJ, Auwerx J. Regulation of PGC-1α, a nodal regulator of mitochondrial biogenesis. *Am J Clin Nutr*. 2011;93(4):884S–8890.
19. He C, Murthy S, McCormick ML, Spitz DR, Ryan AJ, Carter AB. Mitochondrial Cu,Zn-superoxide dismutase mediates pulmonary fibrosis by augmenting H2O2 generation. *J Biol Chem*. 2011;286(17):15597–15607.
20. Xiao W, Wang RS, Handy DE, Loscalzo J. NAD(H) and NADP(H) redox couples and cellular energy metabolism. *Antioxid Redox Signal*. 2018;28(3):251–272.
21. Zhu Y, Dean AE, Horikoshi N, Heer C, Spitz DR, Gius D. Emerging evidence for targeting mitochondrial metabolic dysfunction in cancer therapy. *J Clin Invest*. 2018;128(9):3682–3691.
22. Álvarez D, et al. IPF lung fibroblasts have a senescent phenotype. *Am J Physiol Lung Cell Mol Physiol*. 2017;313(6):L1164–L1173.
23. Pernas L, Scorrano L. Mito-Morphosis: mitochondrial fusion, fission, and cristae remodeling as key mediators of cellular function. *Annu Rev Physiol*. 2016;78:505–531.

24. Rosdah AA, K Holien J, Delbridge LM, Dusting GJ, Lim SY. Mitochondrial fission - a drug target for cytoprotection or cytodestruction? *Pharmacol Res Perspect*. 2016;4(3):e00235.
25. Zhao J, et al. Mitochondrial dynamics regulates migration and invasion of breast cancer cells. *Oncogene*. 2013;32(40):4814–4824.
26. Whelan RS, et al. Bax regulates primary necrosis through mitochondrial dynamics. *Proc Natl Acad Sci USA*. 2012;109(17):6566–6571.
27. Hirschhäuser C, et al. NOX4 in mitochondria: yeast two-hybrid-based interaction with complex I without relevance for basal reactive oxygen species? *Antioxid Redox Signal*. 2015;23(14):1106–1112.
28. Kozieł R, et al. Mitochondrial respiratory chain complex I is inactivated by NADPH oxidase Nox4. *Biochem J*. 2013;452(2):231–239.
29. Bordt EA, et al. The putative Drp1 inhibitor mdivi-1 is a reversible mitochondrial complex I inhibitor that modulates reactive oxygen species. *Dev Cell*. 2017;40(6):583–594.e6.
30. Martinez FJ, Lederer DJ. Focus on idiopathic pulmonary fibrosis: advancing approaches to diagnosis, prognosis, and treatment. *Chest*. 2018;154(4):978–979.
31. Han CY, et al. NADPH oxidase-derived reactive oxygen species increases expression of monocyte chemotactic factor genes in cultured adipocytes. *J Biol Chem*. 2012;287(13):10379–10393.
32. Ullevig S, Zhao Q, Lee CF, Seok Kim H, Zamora D, Asmis R. NADPH oxidase 4 mediates monocyte priming and accelerated chemotaxis induced by metabolic stress. *Arterioscler Thromb Vasc Biol*. 2012;32(2):415–426.
33. Yeligar SM, Harris FL, Hart CM, Brown LA. Ethanol induces oxidative stress in alveolar macrophages via upregulation of NADPH oxidases. *J Immunol*. 2012;188(8):3648–3657.
34. Yu L, et al. Megakaryocytic leukemia 1 bridges epigenetic activation of NADPH oxidase in macrophages to cardiac ischemia-reperfusion injury. *Circulation*. 2018;138(24):2820–2836.
35. Den Hartigh LJ, et al. Adipocyte-Specific deficiency of NADPH oxidase 4 delays the onset of insulin resistance and attenuates adipose tissue inflammation in obesity. *Arterioscler Thromb Vasc Biol*. 2017;37(3):466–475.
36. Shanmugasundaram K, Nayak BK, Friedrichs WE, Kaushik D, Rodriguez R, Block K. NOX4 functions as a mitochondrial energetic sensor coupling cancer metabolic reprogramming to drug resistance. *Nat Commun*. 2017;8(1):997.
37. Gibbons MA, et al. Ly6Chi monocytes direct alternatively activated profibrotic macrophage regulation of lung fibrosis. *Am J Respir Crit Care Med*. 2011;184(5):569–581.
38. Zhou Y, et al. Chitinase 3-like 1 suppresses injury and promotes fibroproliferative responses in Mammalian lung fibrosis. *Sci Transl Med*. 2014;6(240):240ra76.
39. Redente EF, et al. Tumor necrosis factor-α accelerates the resolution of established pulmonary fibrosis in mice by targeting profibrotic lung macrophages. *Am J Respir Cell Mol Biol*. 2014;50(4):825–837.
40. Ashley JW, et al. Polarization of macrophages toward M2 phenotype is favored by reduction in iPLA2β (group VIA phospholipase A2). *J Biol Chem*. 2016;291(44):23268–23281.
41. Satoh T, et al. Identification of an atypical monocyte and committed progenitor involved in fibrosis. *Nature*. 2017;541(7635):96–101.
42. Scott MKD, et al. Increased monocyte count as a cellular biomarker for poor outcomes in fibrotic diseases: a retrospective, multicentre cohort study. *Lancet Respir Med*. 2019;7(6):497–508.
43. Standiford TJ, Kunkel SL, Phan SH, Rollins BJ, Strieter RM. Alveolar macrophage-derived cytokines induce monocyte chemoattractant protein-1 expression from human pulmonary type II-like epithelial cells. *J Biol Chem*. 1991;266(15):9912–9918.
44. Young LR, et al. Epithelial-macrophage interactions determine pulmonary fibrosis susceptibility in Hermansky-Pudlak syndrome. *JCI Insight*. 2016;1(17):e88947.
45. Bernard K, et al. NADPH oxidase 4 (Nox4) suppresses mitochondrial biogenesis and bioenergetics in lung fibroblasts via a nuclear factor erythroid-derived 2-like 2 (Nrf2)-dependent pathway. *J Biol Chem*. 2017;292(7):3029–3038.
46. Kim SJ, et al. CRIF1 is essential for the synthesis and insertion of oxidative phosphorylation polypeptides in the mammalian mitochondrial membrane. *Cell Metab*. 2012;16(2):274–283.
47. Jung SB, et al. Reduced oxidative capacity in macrophages results in systemic insulin resistance. *Nat Commun*. 2018;9(1):1551.
48. Van den Bossche J, et al. Mitochondrial dysfunction prevents repolarization of inflammatory macrophages. *Cell Rep*. 2016;17(3):684–696.
49. Formentini L, et al. Mitochondrial ROS production protects the intestine from inflammation through functional M2 macrophage polarization. *Cell Rep*. 2017;19(6):1202–1213.
50. Murthy S, Larson-Casey JL, Ryan AJ, He C, Kobzik L, Carter AB. Alternative activation of macrophages and pulmonary fibrosis are modulated by scavenger receptor, macrophage receptor with collagenous structure. *FASEB J*. 2015;29(8):3527–3536.
51. Murthy S, Ryan A, He C, Mallampalli RK, Carter AB. Rac1-mediated mitochondrial H2O2 generation regulates MMP-9 gene expression in macrophages via inhibition of SP-1 and AP-1. *J Biol Chem*. 2010;285(32):25062–25073.
52. Mookerjee SA, Brand MD. Measurement and analysis of extracellular acid production to determine glycolytic rate. *J Vis Exp*. 2015;(106):e53464.
53. Osborn-Heaford HL, et al. Mitochondrial Rac1 GTPase import and electron transfer from cytochrome c are required for pulmonary fibrosis. *J Biol Chem*. 2012;287(5):3301–3312.
54. Janssen AJ, et al. Spectrophotometric assay for complex I of the respiratory chain in tissue samples and cultured fibroblasts. *Clin Chem*. 2007;53(4):729–734.